On the smoothing of rough surfaces

1999 J. Phys.: Condens. Matter 11 4349

(http://iopscience.iop.org/0953-8984/11/22/307)

J. Phys.: Condens. Matter **11** (1999) 4349–4365. Printed in the UK PII: S0953-8984(99)01555-6

On the smoothing of rough surfaces

M S Hoogeman†§, M A J Klik†, R van Gastel‡ and J W M Frenken‡‖

† FOM–Institute for Atomic and Molecular Physics, Kruislaan 407, 1098 SJ Amsterdam, The Netherlands

‡ Kamerlingh Onnes Laboratory, Leiden University, PO Box 9506, 2300 RA Leiden, The Netherlands

E-mail: frenken@phys.leidenuniv.nl

Received 2 February 1999

Abstract. We present a study of the annealing of non-equilibrium structures on Ni(001). The non-equilibrium structures are produced by sputtering, and are investigated by scanning tunnelling microscopy. We find that, depending on the precise amount of removed material, the surface morphology evolves towards equilibrium along different pathways. This reflects itself in differences in the large-scale patterns that form and the time and temperature dependences of the restoration processes. We explain these differences in terms of the atomic-scale diffusion mechanisms responsible for the surface mass transport. Two of these pathways, ripening and coalescence of vacancy islands, are studied in more detail. We observe local correlations in Ostwald ripening and find anomalous behaviour of vacancy islands when these are in close proximity to each other.

1. Introduction

The most common method by which metal surfaces are cleaned in an ultrahigh-vacuum environment is ion erosion of the top layers. The low-energy bombardment, e.g. with Ar ions, introduces damage on the surface in the form of mounds and pits. Although the roughness increases dramatically, the crystallinity of the surface is hardly affected [1–4]. The roughness is usually removed by heating the surface to sufficiently high temperatures, so that the surface mobility is high enough to flatten the surface.

Using programmable-temperature scanning tunnelling microscopy (STM) [5], we are able to follow the complete annealing of a damaged surface within one single STM measurement. By varying the sputter dose we find that the completion of the outermost layer is a critical step in the annealing of a surface. The precise amount of material missing from the top layer determines the atomic-scale diffusion mechanism by which the surface evolves to its flat, equilibrium configuration. Evidently, the atomic-scale transport mechanism determines the 'repair time', or correspondingly the 'repair temperature' (section 2.3).

We study one of the transport mechanisms in more detail. In section 3 we investigate the local correlations in the Ostwald ripening of vacancy islands. Vacancy islands in close proximity show anomalous behaviour in vacancy exchange rate and coalescence. This is discussed in section 4.

§ Present address: The Netherlands Cancer Institute/Antoni van Leeuwenhoek Huis, Department of Radiotherapy, Plesmanlaan 121, 1066 CX Amsterdam, The Netherlands.

‖ Author to whom any correspondence should be addressed. Fax: +31 71 5275404.

0953-8984/99/224349+17$19.50

2. Experiment

2.1. Experimental procedures

The Ni(001) sample ($4.9 \times 4.9 \times 2\ \mathrm{mm}^3$) was spark-cut from a high-purity single-crystal ingot. The crystal was chemically etched and mechanically polished, after which it was transferred to the ultrahigh-vacuum chamber. The surface was cleaned *in situ* by a few tens of cycles of Ar-ion sputtering at room temperature and annealing up to 1050 K. To remove the last traces of carbon we exposed the surface to 0.75 L of oxygen prior to annealing. The level of impurities was below the 1% detection limit of Auger electron spectroscopy (AES). After preparation the average terrace width was of the order of 0.2 μm.

The STM tip was prepared by electrochemical etching of a 0.25 mm diameter W wire and directly transferred to the UHV chamber or first annealed in vacuum. The tip was further prepared *in situ* by field electron emission and Ar-ion sputtering.

The STM measurements were performed with the high-speed, programmable-temperature scanning tunnelling microscope [5].

2.2. Preparation of damaged surfaces

After the preparation of a clean and flat surface, we erode the surface by use of the 600 eV Ar-ion beam at room temperature. To achieve different levels of erosion we change the Ar-ion dose by varying the exposure time at fixed beam intensity. The removal of two monolayers (ML) of Ni corresponds with an exposure time of 20 minutes, at an average beam current (primary-ion current plus secondary-electron current) on the sample of $\approx$50 nA (Ar pressure of 1×10^{-5} mbar). The measured current on the sample drops during ion erosion by 10%, which is presumably due to a change of the secondary-electron emission coefficient caused by the increased number of steps on the surface.

Figure 1 shows two STM images measured after the removal of 2 ML. All step heights present on the surface correspond to monatomic steps on Ni(001), indicating that the eroded surface is fully crystalline. The number of different terrace levels lies around 7. Two distinct regions are visible in figure 1(a). The difference in average height between these regions is precisely equal to one monatomic step height on Ni(001), and the direction of the boundary

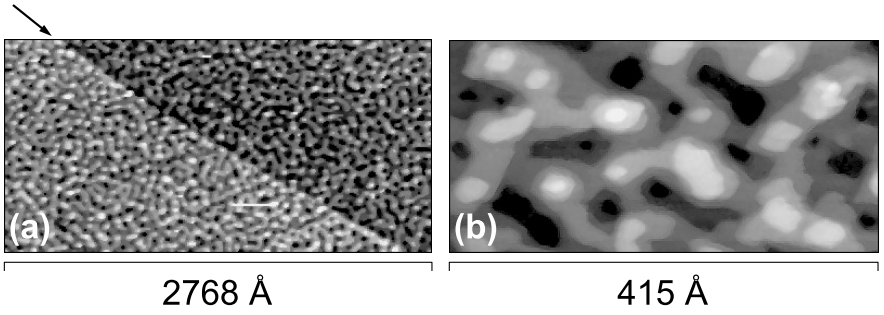

Figure 1. Two STM topographs of a damaged Ni(001) surface measured at room temperature. The images were obtained after the removal of 2 ML of Ni by Ar^+-beam erosion at room temperature. The height variations in both images all correspond to monatomic steps on Ni(001). The two regions in (a) represent two formerly flat (001) terraces, separated by a monatomic step (see the arrow) (2768 Å $\times$ 1384 Å, $V_t = -0.31$ V, $I_t = -0.05$ nA). Image (b) was measured with a larger magnification (415 Å $\times$ 208 Å, $V_t = -0.31$ V, $I_t = -0.05$ nA).

between these regions is perpendicular to the global miscut direction of the crystal. This boundary is a step separating two formerly flat (001) terraces. The fact that monatomic steps 'survive' an ion erosion of 2 ML indicates that the erosion of the surface takes place very locally and very homogeneously.

2.3. Annealing of damaged surfaces

Figure 2 shows a sequence of STM images taken during a temperature ramp of the damaged Ni(001) surface to 550 K. Almost precisely two monolayers of Ni have been removed by ion erosion. Due to the extremely low perpendicular drift of the scanning tunnelling microscope it is possible to monitor the complete repair process over the wide temperature range without mechanical adjustments. Roughly each 300 s we increase the temperature, typically by 10 K. At each temperature raise we observe that after an initial change of the surface, the rate of repair quickly slows down. From room temperature to 363 K the roughness reduces and the lateral length scale of typical surface structures increases. Above 363 K the surface consists of compact ad-islands and vacancy islands. The number of ad-islands and vacancy islands decreases, while the mean sizes of both do not change significantly. At 550 K the annealing of the surface is almost complete.

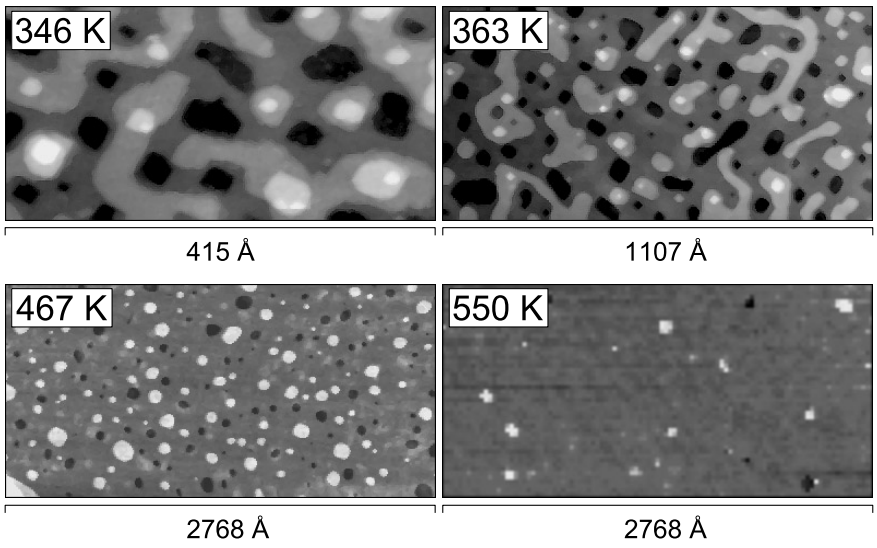

Figure 2. A sequence of STM images of the annealing of a damaged Ni(001) surface. The starting configuration is shown in figure 1. At 467 K the ad-islands and vacancy islands are compact. The anneal process is finished by the exchange of material between ad-islands and vacancy islands and vice versa. At 550 K the surface is nearly flat ($V_t = -0.31$ V, $I_t = -0.05$ nA).

Figure 3 shows a sequence of STM images of the annealing of a surface from which 1.5 ML have been removed. Again, we monitor the complete evolution from a damaged to a flat surface within one single STM measurement. The experiment is performed at the same average heating rate as the one in figure 2. From room temperature to 363 K the evolution is similar to the previous case. For higher temperatures, however, we see a striking difference. While in the previous case the surface evolves to a configuration with compact ad-islands and vacancy islands, here, we observe a connected network of monatomic ridges. The pattern percolates and its lateral dimension scales up with increasing temperature. At 651 K, 100 K

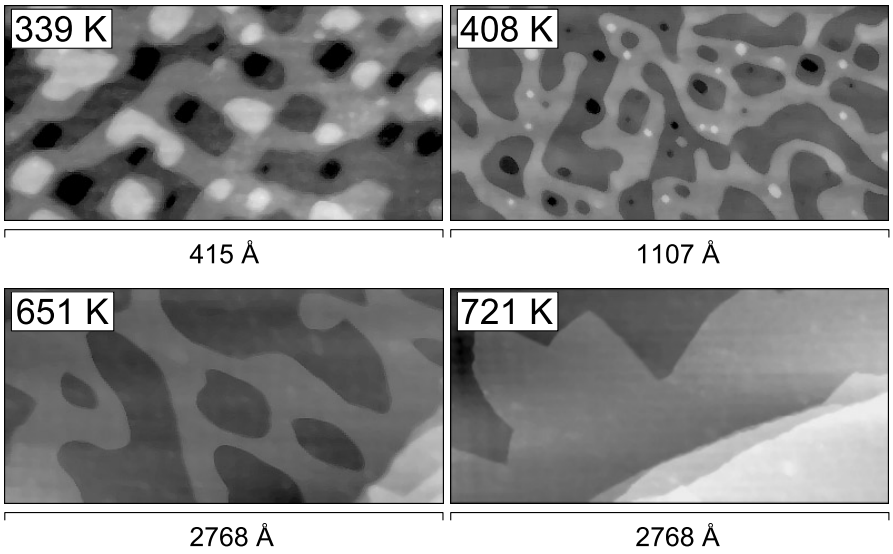

Figure 3. A sequence of STM images of the annealing of a Ni(001) surface, from which 1.5 ML of material is removed. At 408 K a connected pattern of ridges is visible, which coarsens with increasing temperature. When the length scale of this pattern becomes equal to the mean terrace width, the annealing process is complete ($V_t = -1.1$ V, $I_t = -0.05$ nA).

above the last image of figure 2, the network of ridges is still present. At 721 K the typical length scale of the pattern has become equal to the average terrace width, so the annealing to a flat surface is almost complete.

In both experiments the repair of the surface starts with the decrease of the number of levels and an increase of the lateral length scale. This has been observed before, by Michely *et al* [6], for sputtered Pt(111) surfaces. At the atomic scale, adatoms detach from steps and descend to lower terraces. Equivalently, single vacancies are formed at steps of a lower terrace and annihilate at the steps of an upper terrace. The striking difference between the two experiments occurs in the final stage of the repair process, namely the completion of the outermost layer. In figure 2 almost precisely an integer number of monolayers were removed. During the repair of the top layer the material in the ad-islands is simply used to fill up the vacancy islands. In figure 3 the top layer cannot be restored that easily because 50% of that layer is missing. In this case the annealing process is completed when the length scale of the vacancy-island patterns on the surface equals the mean terrace width, so the damage annihilates with the steps. The mean terrace width depends on the global misorientation of the surface normal with respect to the (001) direction. The length scale of an incomplete surface layer evolves through coalescence and ripening. These two processes are much less efficient than the mass transfer from ad-islands to vacancy islands, provided that no additional diffusion barrier at the edge of an island hinders the latter type of transport.

The repair of a damaged surface depends critically on the amount of material in the top layer. It determines the atomic-scale diffusion mechanism by which the annealing of the surface is completed. In figure 4 we summarize the different configurations occurring during the completion of the top layer as a function of the number of removed layers. Figure 4(a) shows the configuration when precisely an *integer* number i of monolayers are removed. In this regime, adatoms detach from ad-islands and diffuse to neighbour ad-islands or vacancy islands. Equivalently, single vacancies are formed at the edges of vacancy islands and annihilate at the

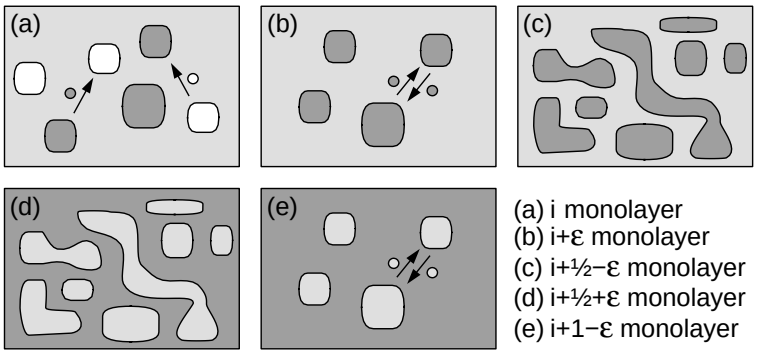

Figure 4. A schematic representation of the different configurations occurring during the annealing of the top layer. (a) Precisely an integer number of layers are removed. Atoms diffuse from ad-islands to vacancy islands and single vacancies diffuse from vacancy islands to ad-islands. (b) Material consisting of slightly more than an integer number of monolayers is removed, which results in the formation of vacancy islands. The surface evolves mainly through Ostwald ripening. (c), (d) Around half of a monolayer is missing. Ripening of islands is combined with coalescence. (d) Material consisting of slightly less than an integer number of monolayers is removed, which results in ad-islands, which evolve mainly through ripening.

edges of ad-islands or are incorporated in surrounding vacancy islands. Vacancies can also form at ad-island edges, as has been demonstrated recently for Cu(001) [7]. Mass transport from ad-islands to vacancy islands and *vice versa* eventually results in the complete annihilation of all islands. This process is the most effective mechanism for restoring the top layer, provided that the Schwoebel–Ehrlich [8, 9] diffusion barrier at the island edges does not block the interlayer diffusion.

Figure 4(b) sketches the configuration in which material consisting of slightly more than an integer number of monolayers is removed. The low density of vacancy islands evolves by exchange of single vacancies (or adatoms). The density of single vacancies around a vacancy island with a small radius is higher than around a vacancy island with a large radius. Consequently, large islands grow at the expense of small islands. This so-called Ostwald ripening will be discussed in section 3. Eventually, all islands disappear, because steps also participate in the ripening process. Steps represent a vacancy or ad-island with an infinite radius. From the STM sequences we conclude that the diffusion and coalescence of the vacancy islands is of negligible importance to the repair process under these conditions. The repair of the top layer by Ostwald ripening is a slow process.

When even more material is removed, the vacancy-island density is increased (figure 4(c)). As the vacancy islands are in close proximity to each other, coalescence events for islands contribute to the annealing of the top layer. In the case of figure 3, the frequency of these events was so high that vacancy islands were not able to reach their equilibrium shape between subsequent coalescence events.

When material consisting of less than an integer number of monolayers is removed, the top layer contains ad-islands instead of vacancy islands (figures 4(d), 4(e)). These two cases are topologically equivalent to the configurations in figures 4(c), 4(b) with single vacancies and vacancy islands replaced by adatoms and ad-islands. Of course, we expect the values of the diffusion barriers to be different.

In summary, the precise amount of material remaining in the topmost layer determines the atomic-scale mechanism which dominates the final annealing stages of the surface. The huge difference between the efficiencies of the different atomic-scale processes makes the necessary

'repair time' and 'repair temperature' depend critically on the deviation of the removed amount from an integer number of monolayers.

3. Ripening of vacancy islands

3.1. Introduction

When we remove slightly more than an integer number of monolayers, the topmost layer is confronted with a deficit of Ni atoms. After the initial annealing stages, the missing material is organized in the form of vacancy islands with a depth of one atomic layer. Figure 5 shows three STM images taken from a STM sequence showing the evolution of such vacancy islands at a temperature of 457 K. In figure 6 we plotted the size of several islands of figure 5 as a function of time. Large islands grow at the expense of small islands, which eventually disappear. Obviously, there is an exchange of small units— e.g. single vacancies or single adatoms—between the vacancy islands. On Cu(001), vacancy diffusion has been shown to be

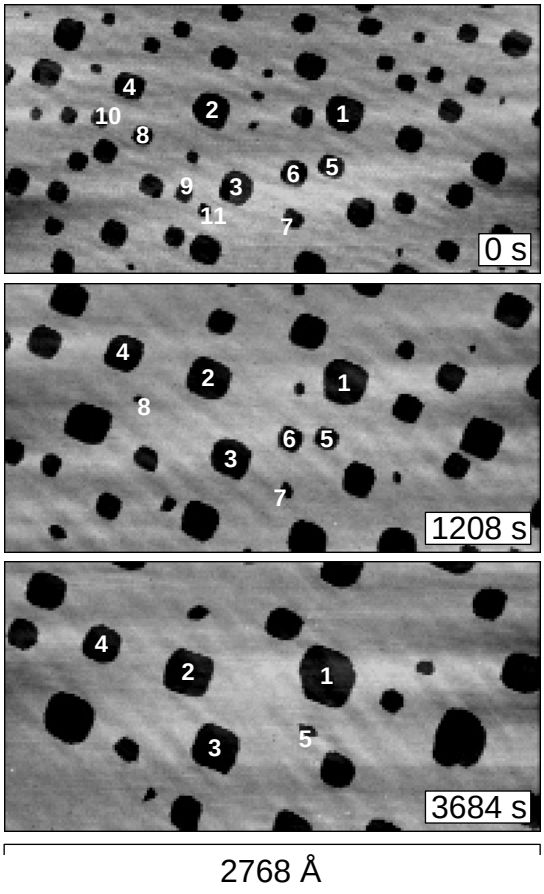

Figure 5. Three STM images from a STM sequence showing the evolution of vacancy islands at 457 K. On average, the large islands grow while the small islands shrink and eventually disappear. Coalescence events for vacancy islands are rare under these conditions (2768 Å $\times$ 1384 Å, $V_t = -0.32$ V, $I_t = 0.03$ nA, imaging time 60.4 s/frame).

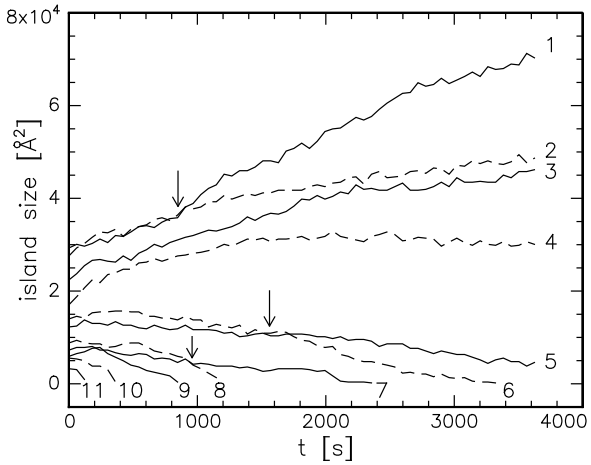

Figure 6. The area of several vacancy islands of as a function of time. The numbers refer to the islands in figure 5. On average, large islands grow and small islands shrink. The arrows indicate several local violations of this 'mean-field' expectation.

the dominant transport mechanism, even between ad-islands [7]. In the remainder of this paper we will describe the exchange in terms of vacancies, but we stress that a completely equivalent description can be given in terms of adatoms. The net vacancy flux towards large islands is positive and for small islands it is negative. This process is known as Ostwald ripening [10].

The theoretical description of Ostwald ripening is based on the Gibbs–Thomson equation:

$$\rho_r = \rho_\infty \exp\left(\frac{\gamma\Omega}{k_B T r}\right) \tag{1}$$

where ρ_r is the equilibrium density of—in this particular case—single vacancies at the edge of an island with radius r, and ρ_∞ is the equilibrium density of vacancies at the edge of a straight step. Ω is the area of a single vacancy, γ is the step free energy per lattice spacing, and k_B and T are the Boltzmann constant and the temperature, respectively. When the equilibrium density ρ_r of vacancies at the island edge is lower than the actual density of its surroundings, the island will grow. When the equilibrium density at the edge is higher, the island will shrink. The rate by which an island changes its area is given by

$$\frac{\mathrm{d}A}{\mathrm{d}t} = -\Omega\kappa(\rho_r - \rho_0) \tag{2}$$

where A is the island area and ρ_0 is the reference vacancy density. The precise definition of the rate factor κ depends on whether or not the diffusion barrier between the terrace and the edge of the island is higher than the usual barrier in the terrace. For a high attachment barrier, $\kappa = 2\pi r D k/a$, where D is the vacancy diffusion constant, k is the factor by which the hopping rate towards the island edge deviates from the rate within the terrace, and a is the lattice spacing. This regime is referred to as the 'attachment-limited' regime. In all other cases the vacancy islands evolve in the 'diffusion-limited' regime, where $\kappa = 2\pi D/\ln l_{sc}$, with the 'screening length' $l_{sc} = R/r$ [11]. The reference vacancy density ρ_0 depends on the size and position distributions of the ensemble of vacancy islands and is sensitive to the presence of steps. In classical ripening theory, ρ_0 is taken as the average value of the equilibrium vacancy densities of all islands. In this 'mean-field' approach, the mean density is obtained from the condition that for a closed ensemble of islands, the total amount of material (or in this case the

amount of missing material) is conserved. In other words, the sum of $\mathrm{d}A/\mathrm{d}t$ (equation (2)) over all islands should be 0. This condition leads to the classical ripening equations of the rate of change of the island radius, for the attachment-limited regime:

$$\frac{\mathrm{d}r}{\mathrm{d}t} = -\frac{kD\rho_\infty\gamma\Omega^2}{ak_BT}\left[\frac{1}{r} - \frac{1}{\langle r\rangle}\right] \tag{3}$$

and for the diffusion-limited regime:

$$r\frac{\mathrm{d}r}{\mathrm{d}t} = -\frac{D\rho_\infty\gamma\Omega^2}{\ln l_{sc}\, k_BT}\left[\frac{1}{r} - \left\langle\frac{1}{r}\right\rangle\right]. \tag{4}$$

For this result, equation (1) has been simplified to $\rho_r \simeq \rho_\infty(1 + \gamma\Omega/k_BTr)$ and $\mathrm{d}A/\mathrm{d}t$ has been replaced by $2\pi r\,\mathrm{d}r/\mathrm{d}t$. The angular brackets denote the ensemble average.

3.2. Local ripening

A close inspection of figure 6 reveals a number of deviations of the evolution of vacancy islands from the expected mean-field ripening behaviour. For example, island '1' grows much more rapidly after $t = 1000$ s than island '2', which starts off at the same size. Several experimental [12–15] and theoretical [16] studies have shown that there are strong *local* variations in the ripening of ad-islands and clusters. Reference [13] shows e.g. that the mean-field ripening theory cannot describe all details of the ripening behaviour of ad-islands on Si(001). Local correlations in the ripening of an island can be reproduced by applying the Gibbs–Thomson equation only to an island's *local* environment. In references [13, 16] the local environment of each island was defined by a Voronoi polygon. The Voronoi polygon consisted of bisecting lines, perpendicular to the lines connecting the island centres. We have adopted a similar scheme, but use the perpendicular bisecting lines to the connecting lines between the island edges. In this way, the Voronoi polygon identifies all points that are closer to the edge of the island within that polygon than to any other island edge.

We use the Voronoi construction to calculate a locally defined reference vacancy density ρ_0. As in the mean-field approach, ρ_0 follows from the mass conservation of the ensemble of islands. However, now the island ensemble is limited to the local environment defined by the Voronoi polygon. Each contribution to the local average is weighted with the length L_i of the polygonal tessellation divided by the circumference L_c of the Voronoi polygon:

$$\frac{\mathrm{d}A}{\mathrm{d}t} + \frac{1}{L_c}\sum_{i=1}^{n} L_i\frac{\mathrm{d}A_i}{\mathrm{d}t} = -\Omega\left[\kappa_r(\rho_r - \rho_0) + \frac{1}{L_c}\sum_{i=1}^{n} L_i\kappa_{r_i}(\rho_{r_i} - \rho_0)\right] = 0. \tag{5}$$

From the solution of this equation we obtain ρ_0 for the attachment-limited regime, and for the diffusion-limited regime. Substituting these into equation (2) we find solutions of the form of equations (3) and (4), but with

$$\frac{1}{\langle r\rangle} \qquad \text{replaced by} \qquad \frac{1}{\langle r\rangle_V} = 2\Big/\left(r + \sum_{i=1}^{n} r_iL_i/L_c\right) \tag{6}$$

for the attachment-limited regime, and with

$$\left\langle\frac{1}{r}\right\rangle \qquad \text{replaced by} \qquad \left\langle\frac{1}{r}\right\rangle_V = \frac{1}{2r} + \frac{1}{2L_c}\sum_{i=1}^{n}\frac{L_i}{r_i} \tag{7}$$

for the diffusion-limited regime.

3.3. Results

We test the validity of equations (3) and (6) by plotting $\mathrm{d}r/\mathrm{d}t$ for the data of figure 6 as a function of either $1/r - 1/\langle r\rangle$ or $1/r - 1/\langle r\rangle_V$. To test equations (4) and (7), we plot $r\,\mathrm{d}r/\mathrm{d}t$ against $1/r - \langle 1/r\rangle$ or $1/r - \langle 1/r\rangle_V$. The resulting four plots are shown in figure 7. If the evolution can be described by one of the four scenarios (attachment/diffusion-limited ripening, mean-field/local approach), the data in the corresponding plot should collapse onto a straight line. From figure 7 we conclude that irrespective of whether the exchange of single vacancies is attachment or diffusion limited, the local approach (equations (6), (7)) describes the observations better than the mean-field theory. Although in the mean-field approach the data roughly show the expected behaviour, the scatter on the data significantly reduces when we use the locally defined ρ_0. Comparing attachment- and diffusion-limited exchange (figures 7(b), 7(d)), we conclude that the observed vacancy-island ripening is in the diffusion-limited regime. This agrees with our expectation that there should not be an additional barrier to a single vacancy being incorporated into a vacancy island.

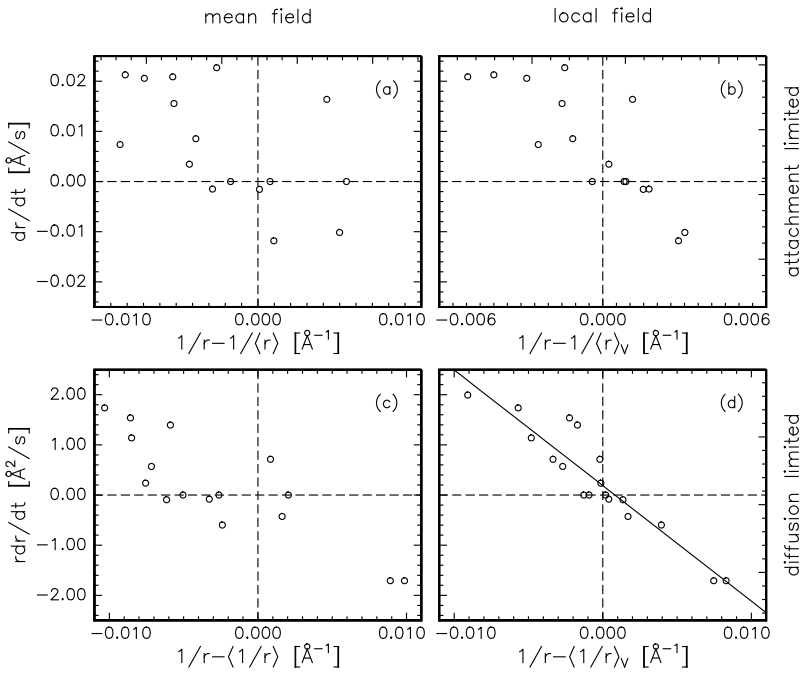

Figure 7. A test of four different ripening scenarios. Each of the four plots contains the same data, obtained from the evolution of islands shown in figure 6. Plots (a) and (c) represent the mean-field description, while (b) and (d) correspond to the local description. The two upper plots (a) and (b) are for attachment-limited vacancy transport and the lower plots (c) and (d) are for diffusion-limited transport. The solid line in (d) is a linear fit to the data.

The prefactor, $D\rho_\infty\gamma\Omega^2/\ln l_{sc}\,k_BT$, of equation (4) is determined from a linear fit to the data of figure 7(d). Substituting in the vacancy area $\Omega = 6.2$ Å^2 and the temperature $T = 457$ K and setting $\ln l_{sc}$ to 1 [10], we obtain $D\rho_\infty\gamma = (3.8 \pm 0.4) \times 10^{-10}$ J m^{-1} s^{-1} at 457 K. Using the step free energy $\gamma = 0.191$ eV/lattice spacing of the (111) step on Ni(001), derived from effective-medium-theory calculations [17], we find a value for the mass-transport coefficient of $(D\rho_\infty)_{457\,\mathrm{K}} = 3.1 \pm 0.3$ Hz, which is one quarter of the frequency with which each site on an extended terrace is 'visited' by a single vacancy.

4. Anomalous behaviour of vacancy islands

4.1. Introduction

Figure 8 shows two STM images of partially annealed surfaces with different fractions of missing material in the top layer. The surfaces were prepared as described in section 2. The total amount of removed material was less than 1 ML in both cases. The surface with the lowest fraction of missing atoms contains an ensemble of vacancy islands in their equilibrium shape. The equilibrium shape is fourfold symmetric with corners which become more rounded with increasing temperature. The evolution of the incomplete layer is dominated by the exchange of single vacancies (or adatoms) between the vacancy islands. On average, the larger islands grow at the expense of the smaller islands [10] (see also section 3 about local Ostwald ripening).

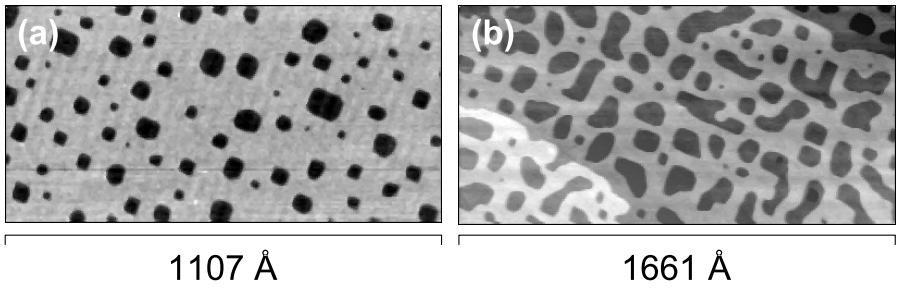

Figure 8. STM topographs measured at 394 K of surfaces partially annealed at that temperature. (a) 17% of the top layer is missing. The vacancy islands exhibit their equilibrium shape and coalescence events are rare (1107 Å × 540 Å, $V_t = 0.79$ V, $I_t = 0.05$ nA). (b) The top layer lacks 30% of Ni atoms. The shapes of the vacancy islands are irregular. Coalescence events dominate the evolution of the surface (1661 Å × 1330 Å).

In figure 9 we plotted the island distance distribution measured from a collection of images obtained under the conditions of figure 8(a) (0.17 ML removed, annealed to 394 K). The distance between the islands was measured from edge to edge. We compare the measured distance distribution with a distribution obtained from random placement of the same vacancy islands. The measured distribution is narrower than the random distribution, and distances below 20 Å are hardly found. Carlow *et al* [14] have shown that the narrowing of distance

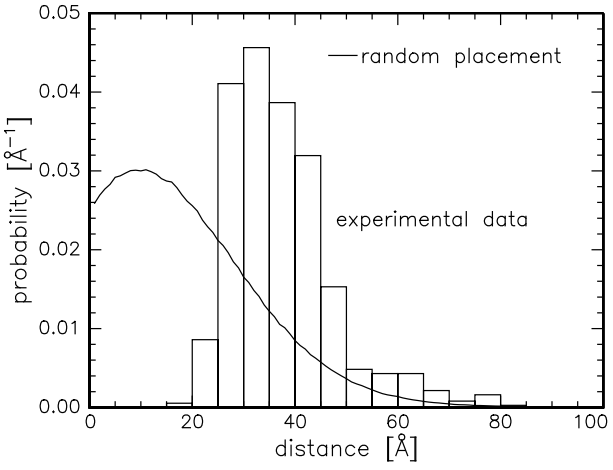

Figure 9. Measured and randomly generated edge-to-edge distance distribution of vacancy islands at 394 K. The random distribution was obtained by a random placement of the vacancy islands from the experimental island distribution under the condition that islands do not overlap.

distributions can be caused by the spatial ordering due to the *local* ripening of islands. If two islands are sufficiently close to each other, they develop a large local gradient in the supersaturation of single vacancies between the islands. Independently of whether the two islands are larger or smaller than the average island size, the smaller of the two will decompose in favour of the larger island. The result is that the probability of two islands being in close proximity reduces and that the spatial distribution is no longer completely random.

If a higher fraction of the outer layer is missing, we find that the vacancy islands have an irregular shape compared with the islands in figure 8(a). From STM sequences of the annealing process we conclude that the irregular shapes are remnants of coalescence events of the vacancy islands. After a coalescence event, the newly formed elongated island does not have enough time to reach its equilibrium shape before being involved in the next coalescence event. The coalescence of vacancy islands dominates the evolution of the surface layer if more than approximately 30% of the outermost layer is removed.

In this section we present a detailed study of vacancy islands which are in close proximity. We show that vacancy islands with an edge-to-edge distance below 20 Å exhibit an anomalous exchange of single vacancies. Furthermore, we studied the coalescence of vacancy islands from STM sequences. We measured the edge-to-edge distance between islands just before coalescence. The average coalescence distance is significantly larger than zero, indicating that at short distances, islands have an anomalously high probability of snapping together. Both phenomena, the anomalous exchange and the anomalous snapping, contribute to the spatial ordering of vacancy islands. We suggest that both phenomena reflect consequences of tensile stress in the Ni(001) surface.

4.2. Anomalous vacancy exchange

Figure 10 shows a fragment of a STM sequence at 434 K, in which two vacancy islands are in close proximity. In the sequence of images the two islands approach each other and rapidly change their size. Eventually, the distance between the island edges increases and the rapid size change stops. In figure 11 we show the sizes of the two islands versus time. Until $t = 2000$ s

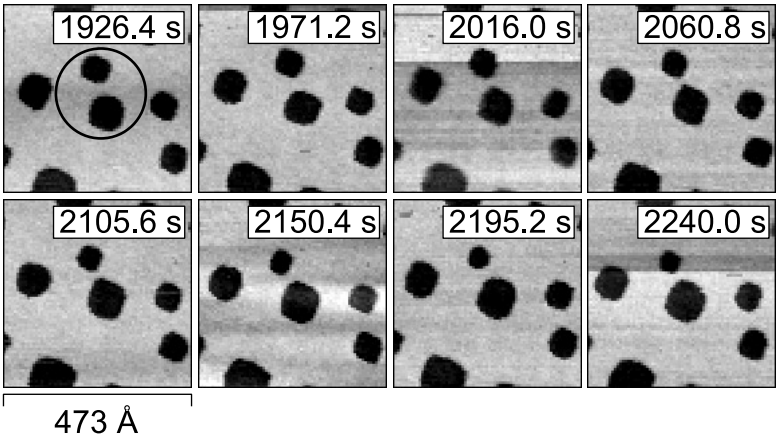

Figure 10. A sequence of STM images from a STM sequence measured at 434 K. The two vacancy islands, marked by the circle, approach each other and change their size rapidly. As long as the two islands are in close proximity, their shape is stretched (473 Å × 492 Å, $V_t = 0.42$ V, $I_t = 0.02$ nA, imaging time 44.8 s/frame).

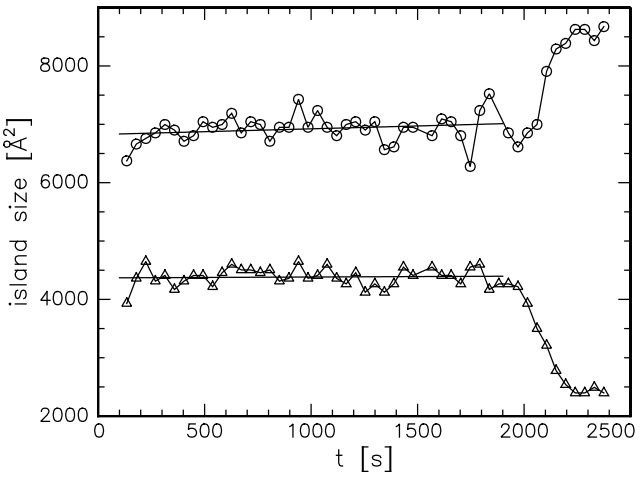

Figure 11. Sizes of the island pair in figure 10 versus time. For $t < 2000$ s the two islands hardly evolve with time. Between $t = 2000$ s and $t = 2250$ s the islands rapidly exchange material. After this period they return to their original, slow evolution.

the rate of change of both islands is close to zero. The larger island shows a minute increase in size, while the size of the smaller island does not change noticeably. This means that the supersaturation of single vacancies around these islands is almost in equilibrium with the local environment. At $t = 2000$ s the rates of change of the two islands suddenly increase by two orders of magnitude. The fact that the smaller island shrinks at the same rate as that at which the large island grows, and with the same total change in the amount of material, shows that the rapid evolution is due to a one-to-one exchange of vacancies (or adatoms) between the two islands.

In figure 12 we plotted from $t = 1400$ s to $t = 2400$ s the edge distance between the two islands, the ratio of the lengths of the two diagonals of the larger island, and again the size of the smaller island. Figure 12 contains several pieces of information. The anomalous exchange starts at edge distances smaller than 25 Å. The edge distances before and during the anomalous exchange differ by less than a factor of 1.4. Thus, the sudden increase of the exchange rate by two orders of magnitude cannot be explained by a simple geometrical argument. For all island couples, for which we observed such an anomalous exchange, we found a threshold distance of 20 ± 5 Å. We did not find a temperature dependence of the threshold distance in the temperature range from 394 K to 473 K.

The second piece of information is contained in the shape change of the islands. As soon as the two islands are within the threshold distance, their shape changes from the equilibrium shape (square with rounded corners) to a stretched one. This shape change is most pronounced for the bigger island. All other islands in the STM sequence keep their equilibrium shape, which excludes the possibility that the shape change is an artifact of the STM observation. If we compare the positions of the two islands with a fixed point on the surface, we find that the nearest three corners of the larger island move towards the smaller island. The furthest corner remains at its original position. There seems to be an attractive force between the edges of the islands which becomes strong enough to deform the islands as soon as the edge distance drops below the threshold distance.

Although it is difficult to decide on the basis of the present data set whether the stretched shape is a thermal shape fluctuation or indeed the result of an attractive force, we nevertheless

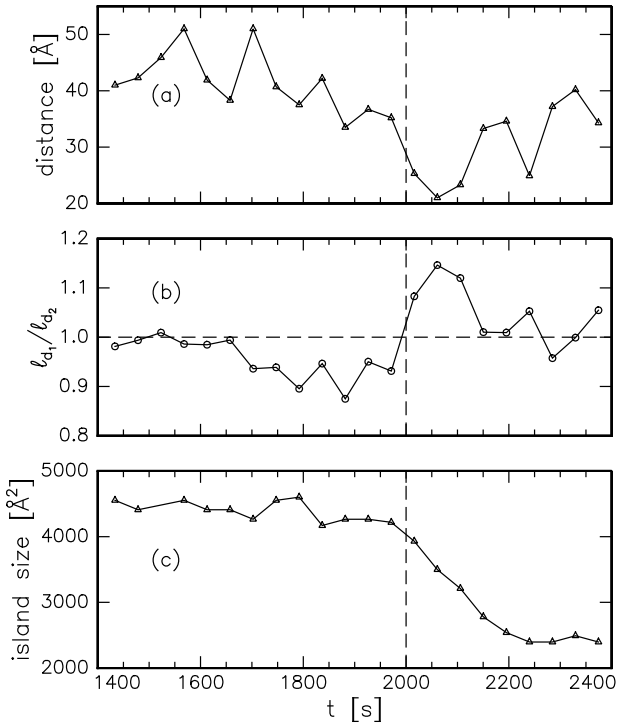

Figure 12. (a) The edge-to-edge distance between the two islands marked in figure 10 as a function of time t. During the anomalous exchange, the distance is below 25 Å. (b) The ratio of the lengths of the two diagonals of the larger island. At $t = 2000$ s the large island stretches out to its smaller neighbour. (c) The size of the smaller island before and during anomalous vacancy exchange.

estimate from the shape change the energy increase of the island. To estimate the possible attraction energy, we determine the free-energy change between the island's equilibrium shape and the observed stretched shape. We assume that the total corner energy is the same for both cases and that the stretching involves the formation of extra kinks and the increase of step length along the two close-packed directions. From the STM images we determine that the increase of step length is 7 Å. This yields an energy change of 0.5 eV, where we used the step free energy $\gamma = 0.191$ eV/lattice spacing. The edges of the stretched island are 10.9° misaligned with respect to the original, close-packed directions. The number of extra kinks is not simply proportional to the tangent of this misalignment angle. The density of thermally excited kinks reduces the number of extra kinks. We compute the density of kinks in a step which is forced to run at angle β with respect to a close-packed direction at a finite temperature at which the density of thermally excited kinks is not negligible. We denote the densities of left-hand and right-hand kinks by p_l and p_r. The difference between the densities is equal to the misorientation of the step:

$$p_l - p_r = \tan\beta. \tag{8}$$

Independently of the misorientation of the step, the product of the densities of left-hand and right-hand kinks should be equal to the Boltzmann weight [18, 19]:

$$\frac{p_l p_r}{(1 - p_l - p_r)^2} = \mathrm{e}^{-2W_0/k_B T} \tag{9}$$

where W_0 is the kink formation energy, k_B the Boltzmann constant, and T the temperature. From equations (8) and (9) we compute the total density of kinks:

$$p_l + p_r = \frac{\sqrt{\tan^2\beta + 4(1-\tan^2\beta)\mathrm{e}^{-2W_0/k_BT}} - 4\mathrm{e}^{-2W_0/k_BT}}{1-4\mathrm{e}^{-2W_0/k_BT}}. \tag{10}$$

The free-energy change is given by

$$\Delta F \simeq (N_{str} - N_{eq})W_0 - k_BT\ln\Omega(N_{str})/\Omega(N_{eq}) \tag{11}$$

where N_{str} and N_{eq} are the average number of kinks of the stretched and original island respectively. $\Omega(N)$ is the total number of configurations with N kinks along the four sides of the island. From the circumference of the island and applying equation (10), we determine that N_{eq} and N_{str} are 5 and 25 respectively. Using equation (11) we arrive at a free-energy change of 1.6 eV, where we used the kink formation energy, $W_0 = 0.154$ eV, predicted by Stoltze [17] from effective-medium-theory calculations. Summing the contributions to the free energy of the increase in step length and the number of extra kinks, we arrive at an energy increase of 2.1 eV of the larger island due to the attraction between the islands.

4.3. Snapping of vacancy islands

Two individual vacancy islands can lower the total step length and number of kinks and consequently the total energy by fusing to one single vacancy island. In the previous section we observed that two islands in close proximity attract each other, although the attraction does not necessarily result in a coalescence of the two islands. To investigate the coalescence behaviour of close vacancy islands in detail we followed coalescence events at a relatively low temperature of 394 K. At this temperature the relaxation time of an island to its equilibrium shape is long enough that the shape of the fused islands contains information about the coalescence event itself.

Figure 13 shows two images of a STM sequence of two islands just before and immediately after coalescence. In the second image a 'corridor' has appeared connecting the two islands. Apart from the corridor, the shape of the fused islands is hardly affected by the relaxation to the new equilibrium shape. We estimate that the distance just before coalescence was at least 26 Å, by comparing the shapes and positions of the small island in the two images. In figure 14 we plotted the edge-to-edge distance distribution of islands just before coalescence. The distribution is obtained by comparing the shapes and positions of fused islands before and after the coalescence. Because the islands immediately start to relax to their new equilibrium shape, the plotted distances are lower estimates of the true edge-to-edge distances. Nevertheless, the distribution is peaked for distances larger than zero, namely 20–30 Å. This suggests that the islands actually *snap* together over a non-zero average distance of at least 20 Å.

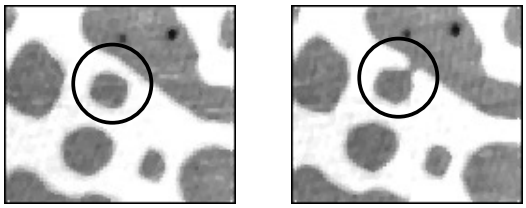

Figure 13. Two STM images from a STM movie of two coalescing vacancy islands measured at 394 K. The two islands snap together over a distance of 26 Å (434 Å × 492 Å, $V_t = 0.42$ V, $I_t = 0.02$ nA; time between images is 57 s).

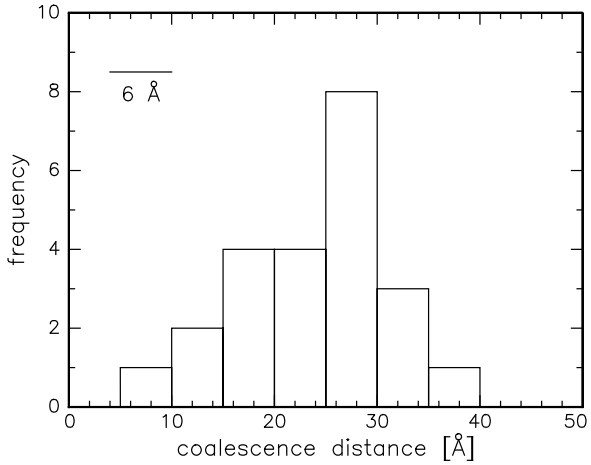

Figure 14. The edge-to-edge distance distribution measured on Ni(001) at 394 K for vacancy islands just before snapping to contact. The distribution shows a clear maximum between 25 and 30 Å. The edge-to-edge distances were obtained from the non-relaxed shapes of the islands before and after snapping and are a lower estimate of the true distance. The size of the horizontal bar indicates the maximum observed distance fluctuation amplitude between neighbouring islands, due to step fluctuations of the individual islands (see figure 15).

The edge distance distribution of figure 14 shows that islands do not coalesce simply by diffusing into each other. Before the islands would 'collide', they have already snapped together. Step fluctuations of the islands might be the responsible for this long-distance snapping. The position fluctuations of the islands edges enlarge the effective size of the island. However, the amplitude of the step fluctuations at 394 K is very modest. In figure 15 we show the edge-to-edge distance between two islands before they snap at $t = 0$ s. Prior to snapping, the distance between the island edges fluctuates with a maximum amplitude of

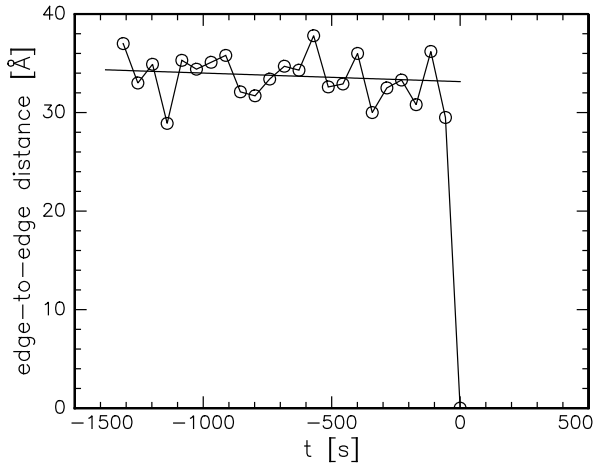

Figure 15. The edge-to-edge distance versus time of two neighbouring islands. The edge-to-edge distance decreases gradually while the island edge positions show modest fluctuations. At $t = 0$ s the islands snap together over a distance of 30 Å.

6 Å. The snap distance of 30 Å is much larger than this fluctuation amplitude. For none of the observed coalescence events did we find evidence that the long-distance snapping was due to the position fluctuations of the island edges.

4.4. Discussion

We have shown that vacancy islands snap together over distances of the order of 25 Å. In addition, islands at small separations exchange vacancies much more rapidly than is expected on the basis of the local supersaturation of single vacancies. Anomalous vacancy exchange was observed for five island pairs which were oriented diagonally with respect to each other, and which were within the threshold distance of 20 ± 5 Å. For one island pair within this distance range we did not find anomalous vacancy exchange. This pair was arranged not diagonally but side to side. We suggest that the island corners play a key role in the exchange mechanism of single vacancies.

The increase of the growth and decay rates implies that the activation energy for vacancy exchange lowers significantly as two island edges approach each other to within 20 ± 5 Å. For islands on top of each other, Giesen *et al* [20] recently reported an increase of mass transport on Cu(111). They found that as soon as the edge of an ad-island touches a descending step of a lower terrace, the decay rate of the ad-island increases by two orders of magnitude. The increased interlayer mass transport was attributed to the disappearance of the Schwoebel–Ehrlich barrier for the diffusion of atoms over steps.

The threshold distance does not depend on temperature in the range from 394 K to 473 K. Schroeder and Wolf [21] have shown that diffusion barriers alter significantly under the presence of elastic fields. Ni(001) is probably under tensile stress [22]. This leads to a strain field around each vacancy island. We suggest that for more or less diagonally placed island pairs the distortion fields around the corners combine to produce a highly (anisotropically) strained channel with a reduced Ni density. Vacancy diffusion through this channel could easily be enhanced by several orders of magnitude. For sufficiently small distances between the corners the strained channel would be mechanically unstable, leading to the rapid formation of the observed corridor, which subsequently relaxes via edge diffusion to give the combined island its final equilibrium shape.

The reason that some island pairs exchange material at an anomalous rate rather than snapping together is not clear. One possibility is that when the initial sizes of the two islands are sufficiently different the transport of vacancies from the smaller to the larger island makes the decrease of the radius of the smaller island larger than the increase of the radius of the larger one. Consequently, the edge-to-edge distance increases, so the anomalous exchange and the probability for coalescence are both reduced.

5. Summary

In this paper we studied the evolution of artificially roughened Ni(001) surfaces. The restoration of the flat surface proceeds in two stages. First, most of the local height differences are removed as the mounds fill up the valleys. This leaves the surface with a net surplus or deficit of atoms in the topmost layer. The pathway along which the topmost layer flattens and the atomic-scale mechanism that governs this evolution depend critically on the amount of material in that layer. The efficiencies of these processes are very different, which leads to huge differences in the necessary ‘repair times’ and ‘repair temperatures’. One of the competing processes is Ostwald ripening of vacancy islands. We showed that the growth or decay rate of each island is determined by its local environment rather than by the mean island size. When two islands

are in close proximity to each other, they display anomalous behaviour. The islands can snap together over a large average distance of 25 Å, and they can exchange vacancies at a rate which is enhanced by two orders of magnitude. These short-distance effects are attributed to the tensile stress of Ni(001).

Acknowledgments

The authors thank R J I M Koper for the preparation of the Ni sample. This work is part of the research programme of the 'Stichting voor Fundamenteel Onderzoek der Materie (FOM)', which is financially supported by the 'Nederlandse organisatie voor Wetenschappelijke Onderzoek (NWO)'.

References

[1] Girard J C, Samson Y, Gauthier S, Rousset S and Klein J 1994 *Surf. Sci.* **302** 73
[2] Teichert Ch, Ammer Ch and Klaua M 1994 *Phys. Status Solidi* a **146** 223
[3] Ritter M, Stindtmann M, Farle M and Baberschke K 1996 *Surf. Sci.* **348** 243
[4] Naumann J, Osing J, Quinn A J and Shvets I V 1997 *Surf. Sci.* **388** 212
[5] Hoogeman M S, Glastra van Loon D, Loos R W M, Ficke H G, de Haas E, van der Linden J J, Zeijlemaker H, Kuipers L, Chang M F, Klik M A J and Frenken J W M 1998 *Rev. Sci. Instrum.* **69** 2072
[6] Michely Th, Land T, Littmark U and Comsa G 1992 *Surf. Sci.* **272** 204
[7] Hannon J B, Klünker C, Giesen M, Ibach H, Bartelt N C and Hamilton J C 1997 *Phys. Rev. Lett.* **79** 2506
[8] Schwoebel R L and Shipsey E J 1966 *J. Appl. Phys.* **37** 3682
[9] Ehrlich G and Hudda F G 1966 *J. Chem. Phys.* **44** 1030
[10] Zinke-Allmang M, Feldman L C and Grabow M H 1992 *Surf. Sci. Rep.* **16** 377 and references therein
[11] At the distance R the vacancy density approaches ρ_0. The ratio between the island radius r and R is assumed to be constant for all islands. The 'screening length' $l_{sc} = R/r$ is introduced as a boundary condition for the vacancy density at finite distance to avoid a logarithmic divergence of the solution of Fick's second diffusion law. Usually, $\ln l_{sc}$ is set to 1 [10].
[12] Theis W, Bartelt N C and Tromp R M 1995 *Phys. Rev. Lett.* **75** 3328
[13] Bartelt N C, Theis W and Tromp R M 1996 *Phys. Rev.* B **54** 11 741
[14] Carlow G R, Barel R J and Zinke-Allmang M 1997 *Phys. Rev.* B **56** 12 519
[15] Rosenfeld G, Morgenstern K, Beckmann I, Wulfhekel W, Lægsgaard E, Besenbacher F and Comsa G 1998 *Surf. Sci.* **402–404** 401
[16] Bartelt M C and Evans J W 1996 *Phys. Rev.* B **54** R17 359
[17] Stoltze P 1994 *J. Phys.: Condens. Matter* **6** 9495
[18] Burton W K, Cabrera N and Frank F C 1951 *Phil. Trans. R. Soc.* A **243** 299
[19] Equation (9) differs slightly from the approximation in reference [18] to make it valid also for high kink densities.
[20] Giesen M, Schulze Icking-Konert G and Ibach H 1998 *Phys. Rev. Lett.* **80** 552
[21] Schroeder M and Wolf D E 1997 *Surf. Sci.* **375** 129
[22] Ibach H 1997 *Surf. Sci. Rep.* **29** 193